Nonlinear Schrödinger flow in a periodic potential

F. Barra,[1] P. Gaspard,[1] and S. Rica[2]
[1]*Center for Nonlinear Phenomena and Complex Systems, Université Libre de Bruxelles, Campus Plaine CP 231, B-1050 Brussels, Belgium*
[2]*Laboratoire de Physique Statistique de l'Ecole Normale Supérieure, associé au CNRS, 24 Rue Lhomond, 75231 Paris Cedex 05, France*
(Received 8 October 1999)

We report a study of solutions of the defocusing nonlinear Schrödinger equation in a spatially periodic potential. The ground-state solution and the steady flows of the system are studied analytically. Above a critical current, a steady state no longer exists and time-dependent solutions are generated, which are numerically simulated and described.

PACS number(s): 42.65.Sf, 05.45.−a, 0.3.75.Fi, 67.40.−w

I. INTRODUCTION

The nonlinear Schrödinger (NLS) equation that describes, among other physical systems, the dynamics of a weakly interacting Bose gas [1,2] has been successfully applied to the interpretation of the experimental observation of trapped condensates [3,4]. Sometime ago it has been proposed as a model of superfluidity due to the existence of a transition from dissipationless flow (superflow) to a dissipative flow. In this transition, energy is removed from the system by the emission from an obstacle, of sound and vortices in the two-dimensional case [5], or of gray solitons in the one-dimensional case [6].

In previous theoretical works [5,6], the obstacles were localized in space. Our aim is to study such a transition in a system with a spatially extended periodic array of obstacles. In particular we consider the NLS flow in a lattice or periodic potential. Applications of this mathematical problem could be found in various systems as we discuss next.

The fast developments in condensate atomic vapors suggest that such an external potential could be imposed by a laser [7]. Actually, it is possible to modify the geometry of the trap to get an almost one-dimensional toroidal Bose-Einstein condensate. Then it is imaginable that several moving laser beams could deplete the condensate density periodically along the condensate. The motion of the laser beams could thus simulate a motion between the periodic lattice and the condensate. This situation will be described by the NLS equation with a periodic potential and the results of the present paper have importance to understand both the stationary and nonstationary properties of the condensate. In fact a similar but simpler experiment has been recently announced by Ketterle and collaborators [7]. They have reported the experimental realization of a superflow passing around one obstacle. As predicted in [5] dissipation appears at a well-defined critical speed.

Applications can also be found in nonlinear optics. In this context, various materials allow the propagation of light pulses without any dispersion because of the nonlinear frequency response of the material to an electromagnetic field [8]. It is reasonable to believe that it is possible to realize a periodic perturbation in the linear refraction index to simulate a periodic potential in the NLS equation.

Moreover, several theoretical works about nonlinear atom optics described in Refs. [9–11] have shown that a NLS type of equation with a periodic potential appears in the description of ultracold atoms interacting with a single standing-wave laser mode or with a traveling laser wave, which might be a further application of our results.

Periodic potential also occurs in crystals. In the superconductivity theory of metals, because of the interaction with the lattice, the electrons form bound pairs that obey Bose statistics. Strictly speaking, a Cooper pair cannot be considered as a bosonic particle because the distance between the two electrons that form the pair can be very big compared to the interatomic distances. Nevertheless for phenomena that vary slowly on the scale of the dimension of the pair (or the coherence length because we are at zero temperature) we can expect an adequate description in terms of a one-particle wave function describing the position of the center of mass of the pair. This description can be used to study the supercurrent when a different crystal of a bigger period is in contact with the superconductor (superlattices). A similar situation arises in superfluid helium flowing in a periodic porous medium.

In this paper we study this problem in a one-dimensional case. The lattice is considered as an external periodic potential of spatial period d', much larger than the interatomic distances. That is we are in the case where one has many particles per cell $nd'^3 \gg 1$, n being the density of particles. We notice that it is not possible to justify such an approach for the case of electric conduction where one has $nd'^3 \sim 1$. However, as we said, our study is applicable to superconduction in a superlattice.

The nonlinear Schrödinger (NLS) equation in one spatial dimension and in the presence of an external nonuniform potential $U(x)$ reads, in a dimensionless form,[1]

[1]Here t, x, ψ, U are dimensionless. In the context of a Bose-Einstein condensate Eq. (1) is obtained from the Gross-Pitaevskiĭ equation by the transformations $t \to \alpha^{-1} t$, $x \to \beta^{-1} x$, $\psi \to \gamma^{-1} \psi$ and for our particular choice of U, $g' \to \delta^{-1} g'$, with $\alpha = [\hbar/2m \times (8\pi a)^2]$, $\beta = 1/8\pi a$, $\gamma = (8\pi a)^{3/2}$, and $\delta = (2m/\hbar^2)(8\pi a)$. Here $2\pi\hbar$ is Planck's constant, m the atomic mass, and a the scattering length. Thus, in the following t is expressed in units of α^{-1}, x in units of β^{-1}, etc., and this defines what we call NLS units.

$$i\psi_t(x,t) = -\psi_{xx}(x,t) + |\psi(x,t)|^2\psi(x,t) + U(x)\psi(x,t). \tag{1}$$

This is a partial differential equation for a complex wave function $\psi(x,t)$. This equation is conservative and Hamiltonian, that is one can write $i\psi_t(x,t) = \delta H/\delta\psi^*$ with

$$H = \int \left(|\psi_x|^2 + \frac{|\psi|^4}{2} + U(x)|\psi|^2 \right) dx. \tag{2}$$

The Hamiltonian dynamics of Eq. (1) preserves, as well as the initial energy H, the initial number of particles $N = \int |\psi(x)|^2\, dx$.

Writing $\psi = \rho^{1/2} e^{i\theta}$, we obtain two ''real'' hydrodynamical fields, ρ and θ, representing, respectively, the particle fluid density and the velocity potential

$$\partial_t \rho = -2\partial_x(\rho\partial_x\theta), \tag{3}$$

$$\partial_t \theta = -(\partial_x\theta)^2 + \frac{1}{\rho^{1/2}}\nabla^2\rho^{1/2} - \rho - U(x). \tag{4}$$

The first equation is the density-mass conservation equation, identifying $2\partial_x\theta$ as the local velocity v. In the second equation, the term $(1/\rho^{1/2})\nabla^2\rho^{1/2}$, often called the quantum pressure is negligible for large scale flows, that is for flows with a space scale much larger than the intrinsic microscopic length ξ_0 (see later). When this quantum pressure is neglected, the equation for θ is the equivalent of Bernoulli's equation for a compressible fluid, with a ballistic equation of state for the pressure (p): $p = \rho^2$.

Actually, for $U(x) \equiv 0$ the ground state is a homogeneous solution: $\psi_0 = \sqrt{\rho_0} e^{-i\rho_0 t}$. On the other hand, long-wavelength and low amplitude perturbations propagate with a sound speed $c_s = \sqrt{2\rho_0}$. $\xi_0 \sim 1/\sqrt{2\rho_0} = 1/c_s$ is the only characteristic microscopic length contained in this equation.

As we said, we shall consider, for simplicity, that the interaction range of the potential $U(x)$ is small compared to its period, so that one may expect to have a ''superflow'' inside each unit cell. The above considerations motivate us to study the NLS equation (1) with the Kronig-Penney potential

$$U(x) = g' \sum_{l=-\infty}^{\infty} \delta(x - ld') \tag{5}$$

with positive g'.

The paper is divided in the following way. First, in Sec. II we look for steady-state solutions. In Sec. II A we discuss the case of pure real wave functions, and in particular the ground state. It will be shown that it is possible to construct an area-preserving nonlinear application of the kind of a Poincaré map that applied to the value and derivative of the wave function in one point of the unit cell gives the value and derivative of the wave function at the corresponding point of the next cell. This map exhibits periodic, quasiperiodic, and chaotic orbits, corresponding to different kinds of spatially extended steady-states solutions.

A similar situation occurs with the discrete Frenkel–Kontorova model where an external periodic potential prevents integrability. In this case, Aubry and Le Daeron [12] have studied in detail the ground-state solutions of the model proving that the ground state can be either periodic or quasiperiodic but not chaotic. They also discuss some particular solutions (discommensurations) which are extrema of the energy but satisfy some particular boundary conditions that distinguish them topologically from the ground states. Here, we will briefly discuss some similar situations.

Then, in Sec. II B, we discuss steady flows, i.e., simple stationary solutions that are not real. We refer to this situation as a flow regime because of the hydrodynamic analogy between the phase of the complex wave function and the speed potential of the Euler equation.

In Sec. III A we present a long-wavelength approximation to describe the sound propagation of the superfluid density variations. A theory for the excitation spectrum in a periodic potential was developed in Ref. [13]. These authors assume a potential with soft variations in order to use a Thomas-Fermi approximation. Here, we study the long-wavelength limit of the excitation spectra but in another limit case, namely, if the potential varies on a very small scale compared to the period of the potential or the interatomic separation. Then, in Sec. III B we show some numerical results to describe the disappearance of the stationary solutions, leading to a dynamical behavior with propagating solitary structures. Finally, in Sec. IV we end with some remarks and conclusions.

II. STATIONARY SOLUTIONS

The stationary solutions of Eq. (1) are the extrema of H with a fixed number of particles, that is, one needs to minimize $H - \mu N$, which gives the following stationary nonlinear Schrödinger equation:

$$0 = -\psi_{xx}(x) - \mu\psi(x) + |\psi(x)|^2\psi(x) + U(x)\psi(x). \tag{6}$$

The chemical potential μ is determined by imposing a finite mean density of particles n

$$n = \lim_{L\to\infty} \frac{1}{L} \int_{-L/2}^{+L/2} dx |\psi(x)|^2.$$

When the obstacle is localized in a finite region of the space, as in [5,6], the asymptotic solution at infinity must be a homogeneous solution with a value $\sqrt{\mu}$, which fixes μ as the asymptotic value of the density. For Eq. (6) this is clearly not the case so that there will be a more complicated relation between μ and the number of particles.

We shall introduce the following dimensionless variables:

$$y = \sqrt{\mu}x, \quad \phi(y) = \frac{\psi(x)}{\sqrt{\mu}}. \tag{7}$$

In these new variables, Eq. (6) reads

$$0 = -\phi_{yy}(y) - \phi(y) + |\phi(y)|^2\phi(y) + \tilde{U}(y)\phi(y), \tag{8}$$

where the external periodic potential is now

$$\tilde{U}(y) = g \sum_{l=-\infty}^{\infty} \delta(y - ld)$$

with the new parameters d and g given by

$$d=\sqrt{\mu}d', \quad g=\frac{g'}{\sqrt{\mu}}. \tag{9}$$

We look for a solution of Eq. (8) of the form $\phi(y)=R(y)\exp i\theta(y)$, putting this form into Eq. (8) one gets the hydrodynamic version of NLS [here $\rho(y)\equiv R(y)^2$]

$$0=-R_{yy}-R+R^3+R\theta_y^2+\tilde{U}(y)R, \tag{10}$$

$$0=\partial_y(2R^2\theta_y). \tag{11}$$

Equation (11) says that a steady current

$$J=2R^2\theta_y \tag{12}$$

is constant through the system. Note, however, that this is the current in the dimensionless variables and is related to the physical current by

$$J_{ph}=\mu^{3/2}J \tag{13}$$

as can be seen from Eqs. (7) and (12). On the other hand, Eqs. (10) and (11) are exactly the equations of motion of a classical Newtonian particle in a central field. In this analogy, the coordinate y plays the role of time, while the constant J is proportional to the angular momentum. Equation (10) becomes

$$0=-R_{yy}-R+R^3+\frac{J^2}{4R^3}+\tilde{U}(y)R, \tag{14}$$

which is the ordinary differential equation for the radial variable $R(y)$. The part $\tilde{U}(y)R$ of the ''force'' depends on the ''time'' y and acts as periodic kicks on the fictitious particle.

A. The ground state and real excitations

Because of the energy (2), it is a general property that the ground-state wave function is real up to a constant phase, let us take then $\theta_y=J=0$. Hence, the wave function satisfies

$$R_{yy}=-R+R^3+g\sum_{l=-\infty}^{\infty}\delta(y-ld)R. \tag{15}$$

(In this section, R is a real wave function and can take positive and negative values.) This Hamiltonian evolution is integrable for $g=0$ in which case

$$c=R_y^2+V(R) \tag{16}$$

is a constant of motion and

$$V(R)=R^2-\frac{R^4}{2} \tag{17}$$

is the ''mechanical'' potential energy. The phase portrait of this integrable system is characterized by two fixed points $R=\pm 1, R_y=0$ for $c=\frac{1}{2}$, unbounded trajectories for $c>\frac{1}{2}$, half-bounded trajectories for $c<\frac{1}{2}$, periodic motions for $0<c<\frac{1}{2}$, and two heteroclinic orbits for $c=\frac{1}{2}$ that connect the aforementioned unstable fixed points.

When $g\neq 0$ the system is perturbed by periodic kicks which break the integrability of the system. The value of c defined in Eq. (16) changes at each kick but takes a constant value c_l over each interval $y\in[ld,(l+1)d]$ where the system is integrable. Equation (15) can be solved in each of these intervals; the solution is formally

$$y=\int_{R(ld)}^{R(y)}\frac{du}{\sqrt{c_l-V(u)}}. \tag{18}$$

Note that this integral is defined only up to a maximum of $R(y)$, that is whenever the square root in the denominator vanishes. The full solution $R(y)$ in the interval is constructed by reflection of the actual solution up to $(l+1)d$. The whole solution for all y is obtained by imposing at each $y=ld$ the continuity of the wave function and a jump condition on the derivative of R which is obtained directly after an integration of Eq. (15) in a small interval around $y=ld$. This condition reads

$$R_y(ld^+)-R_y(ld^-)=gR(ld). \tag{19}$$

$R_y(ld^+)$ is the value of the derivative of R just after $y=ld$ and $R_y(ld^-)$ is the value of the derivative of R just before $y=ld$. Using Eqs. (18) and (19) we can construct a stroboscopic or Poincaré map

$$[R((l+1)d),R_y((l+1)d^+)]=\mathcal{M}[R(ld),R_y(ld^+)]. \tag{20}$$

This map has the symmetry $(R,R_y)\rightarrow(-R,-R_y)$. Owing to the Hamiltonian nature of the evolution, this map has the symplectic property. Maps with this property have also been studied in other situations where the space plays the role of time [12]. The map obtained in Ref. [12] is the standard map, which has properties similar to those of the map (20). However, this similarity is only for the bounded trajectories. Moreover, in the standard map the variable is an angle and thus it must be considered as varying modπ. In our case since the potential decreases to minus infinity the unbounded trajectories diverge in a finite time.

As we know from the properties of the map (20), the typical solutions are either *periodic*, *quasiperiodic*, or *chaotic*. For example, one can easily predict the existence of *periodic* solutions according to the following reasoning. Any periodic solution of the integrable case ($g=0$) which vanishes at each point ld will be the simplest periodic solution of Eq. (6) because, firstly the equation is automatically satisfied and secondly, there is no jump in the derivative R_y since $R(ld)=0$. We notice that this means that such solutions are independent of g. The period could be $\lambda=2d/l$ with l integer. Let us, moreover, note that there is a minimum period that equals 2π [2] determined by the internal scale in the free NLS equation [i.e., $U(x)=0$] known as the healing length.

These periodic orbits appears as points in the R_y axis of the phase portrait. Of course the trivial solution $(R=0,R_y=0)$, is also a *periodic* orbit. For some values of the parameters, these periodic orbits are elliptic and we observe *quasiperiodic* orbits around them. There are other periodic orbits which are hyperbolic. These orbits are connected to

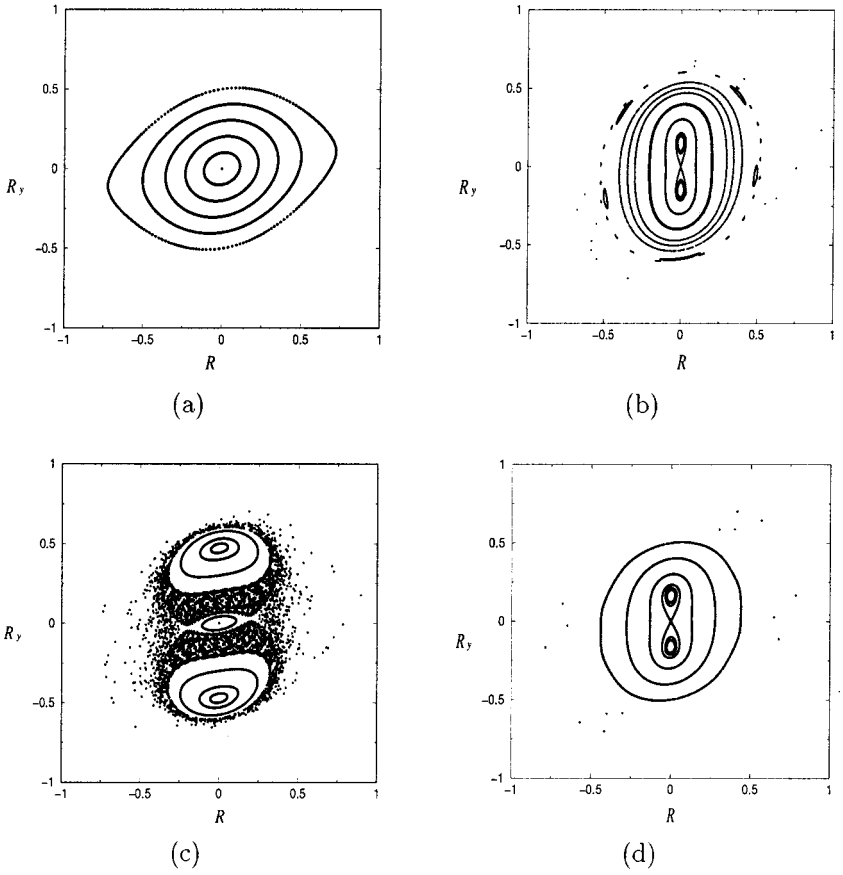

FIG. 1. Nonlinear Poincaré map (20). The quantities are in NLS units (see text). We have taken $g=0.3$ and we change d. (a) Here $d=1>d_c\approx 0.298$. We see the elliptic point at the origin and some quasiperiodic orbits. The quasiperiodic orbits of the map become more and more distorted and collapse into two heteroclinic orbits connecting two hyperbolic points which are not explicitly plotted. (b) Plot for $d=3.17>\pi$. We see that the origin is a hyperbolic point and we can also see the homoclinic orbit. (c) Here $d=3.5>\pi+d_c$; the origin is now elliptic and we observe a sea of chaotic trajectories. We also clearly note two hyperbolic points analogous to the ones appearing in case (a) but here corresponding to a periodic solution of period $\lambda=2d$. (d) For $d=6.35>2\pi$, the origin is again hyperbolic and there is a pair of homoclinic orbits.

homoclinic orbits. Near them, due to the Birkhoff theorem [14], there should exist *chaotic* trajectories.

The pictures in Fig. 1 illustrate the behavior of the map when we vary d in Eq. (15). We can describe the following bifurcation scenario for a small fixed value of g ($=0.3$ in Fig. 1). For $d\in(0,d_c)$ the only fixed point (periodic orbit) is the trivial solution $(R=0,R_y=0)$ which is hyperbolic. At $d=d_c$ there is an inverse pitchfork bifurcation and two hyperbolic fixed points bifurcate from the origin while the trivial solution $(R=0,R_y=0)$ becomes elliptic [see Fig. 1(a)]. In Sec. II A 1 we shall compute d_c and we give a physical interpretation of this bifurcation. There we also show that $d_c<\pi$.

The next change occurs for $d=\pi$, where a new stable periodic orbit bifurcates from the origin while the origin becomes unstable, i.e., the origin undergoes a period-doubling bifurcation. The two points of the new periodic orbit are located on the R_y axis and represent the periodic solution of period $\lambda=2d$ discussed before, i.e., it satisfies $R(ld)=0$. There is a homoclinic orbit which starts (and arrives) at the origin contouring the two points [see Fig. 1(b)].

At $d=d_c+\pi$, another bifurcation occurs. The origin again becomes stable and a new hyperbolic periodic orbit appears [see Fig. 1(c)]. This bifurcation is similar to the one that happens at d_c [see Fig. 1(a)].

In fact, there is a succession of bifurcations of the origin that occur at $d=d_c+l\pi$ (with $l=0,1,2,\ldots$), as we show in Sec. II A 1, which are all equivalent and alternate with bifurcations of the origin at $d=l\pi$ (with $l=1,2,\ldots$). Each one of these latter bifurcations introduces a periodic solution of period $\lambda=2d/l$ [see Fig. 1(d) showing the bifurcation after $d=2\pi$].

We shall see that $d_c\to 0$ when $g\to 0$. So for $g=0$ the origin is unstable only for $d=l\pi$. This can also be obtained by linearizing Eq. (15) around zero and computing the monodromy matrix A which evolves the system over one period. It is easy to see that $\mathrm{Tr}\,A=2\cos d$. Since the stability condition reads $|\mathrm{Tr}\,A|<2$ [15], we see that instability occurs for $d=l\pi$. The curves $d=l\pi$ and $d=d_c(g)+l\pi$ in the plane $d-g$ determine stability regions which are typical of parametric instability.

1. The ground state

For $g=0$ the ground state is $[R(y),R_y(y)]=[\pm 1,0]$ and is represented by two fixed points. As g increases the ground state is a perturbation of this uniform state. The fact that the external potential is repulsive suggests a solution of the form depicted in Fig. 2.

This periodic solution is exactly the one characterized by the unstable fixed point of the map (20) which appears for $d>d_c$ and which is located outside the elliptic island of Fig. 1(a). Moreover, it is the only real solution without zeros as expected for the ground state of a convex energy functional [see Sec. IV B for the convexity and properties of this functional],

$$E[R(\cdot),R_y(\cdot)]=\mu^{3/2}\int\left(|R_y(y)|^2+\frac{|R(y)|^4}{2}+g\sum_l\ \delta(y-ld)|R(y)|^2\right)dy. \quad (21)$$

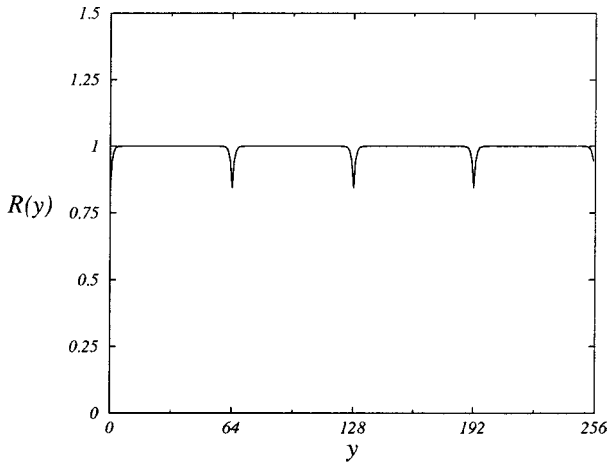

FIG. 2. Numerical calculation of the ground state. The quantities are in NLS units. Here we have used $g'=0.3$, a system with 256 mesh points and periodic boundary conditions. The distance between the deltas is $d=64$ mesh points. The mesh size being $dy=1$. We use a relaxation method to find the local minima of the functional associated with Eq. (6) with a given μ and homogenous initial condition.

This energy gets its minimal value at the periodic solution given by the fixed point. Therefore, the ground state satisfies

$$c_l = c \quad \forall \ l, \tag{22}$$

which implies

$$R(ld) = R_0 \quad \forall \ l \tag{23}$$

together with

$$R_y(ld^+) = -R_y(ld^-) = \frac{g}{2} R_0 \quad \forall \ l. \tag{24}$$

The last equality (24) follows directly from Eq. (22) by using Eq. (23) and the condition (19).

The ground state can thus be expressed as

$$y = \int_{R_0}^{R(y)} \frac{du}{\sqrt{c - V(u)}}. \tag{25}$$

R_0 can be written as a function of c using Eqs. (16), (17), and (24)

$$R_0 = \sqrt{1 + \frac{g^2}{4} - \sqrt{\left(1 + \frac{g^2}{4}\right)^2 - 2c}}. \tag{26}$$

In order to determine this solution we should fix the constant c. The symmetry of the solution implies that the function has a maximum at the values $y = ld + d/2$. We can solve the equation $R_y(y) = 0$ with the help of Eq. (16) and we get that the maximum of R takes the value

$$R_{max} = \sqrt{1 - \sqrt{1 - 2c}}.$$

Imposing that this value should be reached at $y = ld + d/2$ we obtain from Eq. (25) the required equation for c

$$\frac{d}{2} = \int_{R_0(c)}^{R_{max}(c)} \frac{du}{\sqrt{c - V(u)}} = I(c). \tag{27}$$

The right-hand side of Eq. (27) is an increasing function of c with its minimum at $c=0$ and a divergence at $c=\frac{1}{2}$ [see Fig. 3(a)]. For values of d smaller than a critical value given by

$$\tan\left(\frac{d_c}{2}\right) = \frac{g}{2} \tag{28}$$

the periodic orbit does not exist. Above this value, this orbit always exists. This is the first bifurcation which occurs by increasing d because we can see from Eq. (28) that it is always smaller than π.

For given d' and g' (the physical parameters of the system) Eq (27) gives the function $c = c(\mu)$ plotted in Fig. 3(b). Equation (28) defines in fact a critical value of μ

$$\tan\left(\frac{d'\sqrt{\mu_c}}{2}\right) = \frac{g'}{2\sqrt{\mu_c}}. \tag{29}$$

We can see that the number of particles N vanishes at $\mu = \mu_c$. Using Eq. (16) we can compute for the ground state the number of particles in each cell as

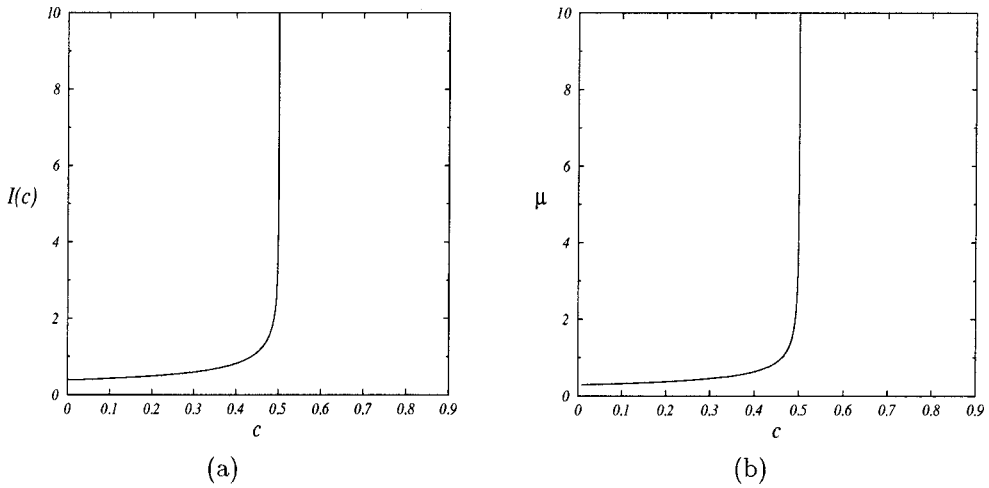

FIG. 3. (a) Plot of the function $I(c)$. (b) μ as a function of c for $g'=0.3$ and $d'=1.0$. The quantities are in NLS units.

$$N=2\sqrt{\mu}\int_{R_0}^{R_{max}}\frac{u^2\,du}{\sqrt{c-V(u)}} \tag{30}$$

which can be evaluated in the limit $\mu\to\mu_c$ giving

$$N=\frac{d'\mu_c c(\mu)}{2}\left(1+\frac{\sin d'\sqrt{\mu_c}}{d'\sqrt{\mu_c}}\right). \tag{31}$$

Here $c(\mu)$ vanishes at μ_c. Thus this bifurcation simply tells us that there is a finite number of particles that can go to the ground state if $\mu>\mu_c$.

2. Real excitations

In the preceding Sec. II A 1, we have identified the ground state with the periodic solution (of period d), which appears after a bifurcation at $d=d_c(g)$. Periodic orbits of period d appear at every $d=d_c(g)+2l\pi$ with $l=1,2,\ldots$, as we can see from Eq. (28). These orbits have exactly $2l$ nodes per unit cell and thus represent excited states.

We have seen that the origin also bifurcates at every $d=d_c(g)+(2l+1)\pi$ with $l=0,1,\ldots$. These orbits are periodic orbits of period $2d$ and they have exactly $2l+1$ nodes per unit cell. To show that $d=d_c(g)+\pi$ is a critical value, we do a calculation similar to the one done in Sec. II A 1. Here the periodic orbit has a node in the middle of the unit cell and is an odd function with respect to that point. The shape of the orbit in the second cell is obtained by reflection of the shape in the first cell. That is we have again that condition (19) is given by Eq. (24) and thus the value of the function at the points ld is given by Eq. (26). Since at $d/2$ the function as a node we have from Eq. (18),

$$\frac{d}{2}=\int_{R_0(c)}^{R_{\max}(c)}\frac{du}{\sqrt{c-V(u)}}+\int_0^{R_{\max}(c)}\frac{du}{\sqrt{c-V(u)}}.$$

Taking the limit $c\to 0$ one gets $g/2=\tan[(d_c+\pi)/2]$. From this equation we see that a periodic orbit (of period $2d$) appears at every $d=d_c(g)+(2l+1)\pi$.

For a given set of the physical parameters, d',g',N, the ground state is a periodic solution which has a value of μ fixed by Eq. (30). Now the excitations of this ground state have different values of μ and they appear in different plots similar to the one in Fig. 1. Therefore, it is difficult to characterize and compare the excitations of a particular system from the map. Nevertheless, from very general properties of this map and because of the Birkhoff theorem [14], we know that each one of the aforementioned orbits represents a physical excitation of the system.

We can argue that these excitations are unstable. To see this we note that, in the absence of an external potential, Eq. (1) is equivalent to the transport equations for the density $\rho=|\psi|^2$ and the mass current $J=i(\psi\psi_x^*-\psi^*\psi_x)$

$$\partial_t\rho+\partial_x J=0.$$

The momentum conservation reads

$$\partial_t J+\partial_x T=0$$

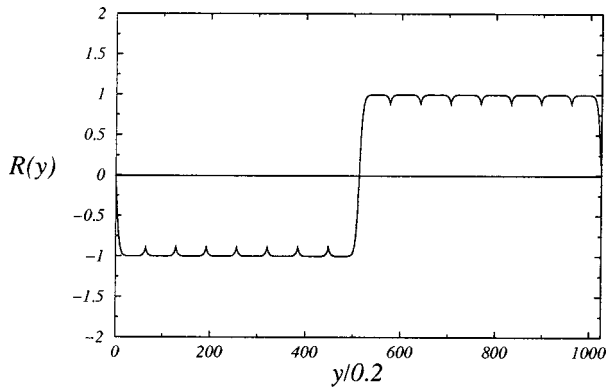

FIG. 4. Numerical simulation of the heteroclinic first excited state. The quantities are in NLS units. Here we have used $g'=0.3$, a system with 1024 mesh points and periodic boundary conditions. The distance between the deltas is $d=64$ mesh points. The mesh size is $dy=0.2$. We have started with an initial condition such that the real part of the wave function changes its sign in an arbitrary point. The imaginary part is zero. We use a relaxation method to find the local minima of the functional associated with Eq. (6) with a given μ. We have noticed that the zero of the wave function moves to the nearest delta external potential. This is natural because the energy contribution of the deltas is $g'\mu\Sigma_l R(ld)^2$; then this energy is lowered as the wave function vanishes in one point ld.

where the flux of momentum T is $T=|\psi|^4-(\psi^*\psi_{xx}+\psi\psi_{xx}^*)+2\psi_x\psi_x^*$. Therefore, the force F acting on a point $y=ld$ of the obstacles is $F=T(ld^+)-T(ld^-)$. For the real steady excitations we have $T=\mu^2R^4-2RR_{yy}+2R_x^2)$ and $R_{xx}=-R+R^3$ so that $T=2c\mu^2$. We see that each point of our obstacle (i.e., on $y=ld$), is submitted to a force $F=2(c_{l+1}-c_l)\mu^2$. This result is quite interesting because it says that the net force on a delta vanishes whenever one has a single integration constant c for all the cells as for the ground state [see Eq. (22)]. We can expect that excitations with different c_l decay because for any perturbation the system will try to minimize this excess of energy and to reach the lower energy state.

A very simple excited state (which is topologically stable whenever we impose a pure real wave function) is the one described by the heteroclinic trajectory joining the two possible fixed points (see Fig. 4). This excited state may be seen as a kink connecting the two different fixed points (ground states) in the map of Fig. 1(a). For low values of g, this wave function has only one zero, so that it is just the lower excited real steady state.

This lower excited steady state is characterized as follows: let $R^{(0)}(y)$ be the ground-state solution in a cell defined by the same constant c at each interval. Let us try the Ansatz $R(y)=A(Y)R^{(0)}(y)+b(y)$, where $A(Y)$ is a slowly varying amplitude. The variable Y denotes this scale of variation $Y\gg d$, so that spatial derivatives must be understood as $\partial_y\to\partial_y+\partial_Y$. We use that the equation for the function $R(y)$ is Eq. (15). One has that the equation for the correction $b(y)$ is

$$\mathcal{L}_A b(y)=\partial_Y^2A(Y)R^{(0)}(y)+2\partial_Y A(Y)\partial_y R^{(0)}(y)+[A(Y)-A(Y)^3]R^{(0)}(y)^3,$$

with

$$\mathcal{L}_A = -\partial_y^2 - 1 + 3A(Y)^2 R^{(0)}(y)^2$$

being a self-adjoint operator with the usual scalar product in the unit cell $\langle f(y)g(y)\rangle = \int_0^d f(y)g(y)dy$.

Finally, the solvability condition for $b(y)$ leads for the mean field equation for the slowly varying amplitude $A(Y)$:

$$\mathcal{D}(A)\partial_Y^2 A(Y) + [A(Y) - A(Y)^3] = 0, \tag{32}$$

where $\mathcal{D} = \langle R^{(0)}(y)\chi_A(y)\rangle / \langle [R^{(0)}(y)]^3 \chi_A(y)\rangle$ and $\chi_A(y)$ belongs to the kernel of $\mathcal{L}_A$. The solution of Eq. (32) is a solution going from $A=+1$ to $A=-1$, slightly different from the usual hyperbolic tangent because $\mathcal{D}_A$ depends explicitly on A. The size of the core is related to the mentioned $\mathcal{D}_A$.

B. Steady flows

Now we turn into the stability of the ground-state solutions when a constant current is imposed on the system. The starting point is Eq. (14) and we look for solutions of this equation that converge to the ground state in the limit $J \to 0$. We proceed as before. In intervals $y \in [ld,(l+1)d]$, the quantity

$$c = R_y^2 + V_J(R) \tag{33}$$

takes a constant value, where

$$V_J(R) = R^2 - \frac{R^4}{2} + \frac{J^2}{4R^2}.$$

The solution can be obtained in the same way as before,

$$y = \int_{R(ld)}^{R(y)} \frac{du}{\sqrt{c_l - V_J(u)}}, \tag{34}$$

where c_l is the value of Eq. (33) in the interval $y \in [ld,(l+1)d]$. $R(ld)$ and c_l are determined from c_{l-1} and $R((l-1)d)$ by the relation

$$R_y(ld^+) = gR(ld) + R_y(ld^-), \tag{35}$$

by the continuity of the function R, and by the solution (34) in the previous interval.

As a particular case, this solution can be periodic imposing $c_l = c, \quad \forall\ l$. At each $y = ld$, the amplitude R takes the same value, we call it R_0. The absolute value of the derivative from the right-hand side is equal to the absolute value of the derivative from the left-hand side, let us call it R_0'. Then the condition (35) reads $R_0' = (g/2)R_0$, and from Eq. (33) we get

$$c(R_0) = \frac{g^2}{4} R_0^2 + V_J(R_0). \tag{36}$$

The maximum of R should again be reached at the values $y = nd + d/2$. The maximum value R_m satisfies

$$c = V_J(R_m) \tag{37}$$

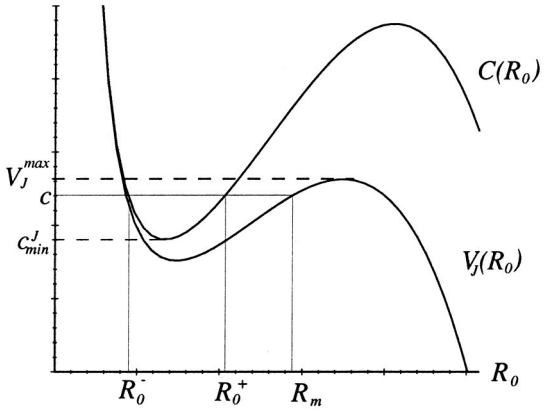

FIG. 5. The effective potential $V_J(R_0)$ and Eq. (36) for $c(R_0)$. The quantities are in NLS units.

so that the undetermined constant c is fixed by the condition

$$\frac{d}{2} = \int_{R_0}^{R_m} \frac{du}{\sqrt{c - V_J(u)}}. \tag{38}$$

It is easy to see that, when $J \to 0$, this solution coincides with the ground state. In terms of a mechanical problem, we have a particle that moves under the effect of the potential V_J (see Fig. 5).

The periodic orbit exists if $V_J^{min} < c < V_J^{max}$, where V_J^{min} and V_J^{max} are the minimum and maximum of the potential, respectively. As the current J increases the difference $V_J^{max} - V_J^{min}$ decreases and there is a value J_q beyond which no periodic orbit exists. This critical value is determined by the condition that the maximum and minimum of the potential merge in the inflection point given by

$$\left.\frac{d}{dR} V_J(R)\right|_{R^*} = 0, \quad \left.\frac{d^2}{dR^2} V_J(R)\right|_{R^*} = 0. \tag{39}$$

These relations allow us to obtain

$$J_q = \frac{4}{3\sqrt{3}} \tag{40}$$

and $R^* = \sqrt{2/3}$. Note that J_q / R^{*2} is exactly the sound speed for a density R^{*2}. No periodic solution exists with currents larger than J_q.

Now we will show that for a fixed set of the parameters g', d', N, a smaller critical value is found. We consider Eq. (38) with a fixed value of J, d, g. As we said, R_0 is a function of c given by Eq. (36). In Fig. 5 we plot $c(R_0)$ and $V_J(R_0)$. A periodic solution exists if $c_{min}^J < c < V_J^{max}$ and for each value of c there are two periodic solutions that correspond to the two possible values of R_0. We shall call R_0^+ the right branch and R_0^- the left branch. This means that there are two possible values for the right-hand side of Eq. (38),

$$\frac{d}{2} = I_{\pm}^J(c), \tag{41}$$

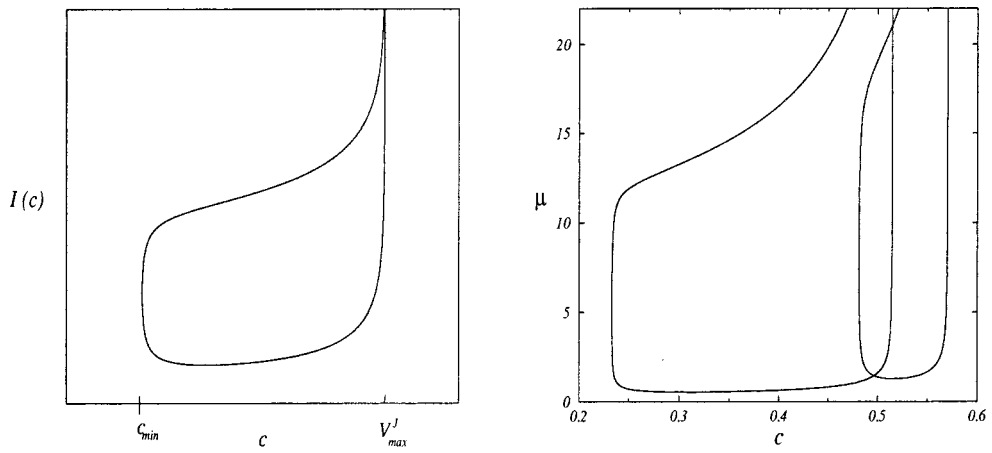

FIG. 6. (a) Schematic plot of $I^J_{\pm}(c)$ as a function of c. (b) Plot of μ as a function of c. The plot is obtained numerically from Eq. (42) for $J=0.24$ and 0.52. One sees from the figure that for a given number of particles, i.e., a given μ^*, the stationary solution disappears if the minimum $\mu_{crit}(J)$ of the curve is greater than this given μ^*. This happens when J increases because the minimum $\mu_{crit}(J)$ increases with J (see text). The quantities are in NLS units.

where $I^J_{\pm}(c)$ is the integral in Eq. (38) starting at $R_0^{\pm}$, respectively [16]. Let us consider $I^J_+(c)$. This function is defined for $c^J_{min}<c<V_J^{max}$. Starting at $c=c^J_{min}$ we see that $I^J_+(c)$ decreases when c increases. In fact, since $c(R_0)$ takes a minimum value a small increase Δc gives a change $\Delta R_0 \sim +\sqrt{\Delta c}$ and a change $\Delta R_m \sim \Delta c$. That is, the integration interval diminishes as $\sqrt{\Delta c}$. Since the integrand also changes at the order Δc we see that $I^J_+(c+\Delta c)$ decreases by an amount of $\sqrt{\Delta c}$ up to leading order. On the other hand, when c is near V_J^{max} the function $I^J_+(c)$ increases. This can be shown by a similar argument using the fact that $V_J(R)$ has a maximum so that a variation Δc on c changes R_m by an amount $\sqrt{\Delta c}$. Therefore $I^J_+(c)$ decreases until a minimum at a value $\tilde{c}(J)$ and then increases up to infinity at $c=V_J^{max}$. On the other hand, it is easy to see that $I^J_-(c)$ always increases and diverges also at $c=V_J^{max}$.

In Fig. 6(a) we plot $I^J_{\pm}(c)$. In terms of the mechanical problem of a particle in the potential V_J, $I^J_{\pm}(c)$ represents the time taken by the particle starting from $R_0^{\pm}$ to arrive at R_m. We know that this time is infinite when the particle has to arrive at a maximum of the potential with zero velocity.

Let us return to our physical problem. In a similar way, as in the case of the ground state, Eq. (41) gives here a relation between μ and c, i.e., $\mu=\mu(c,J)$. This function has a minimum which defines a critical value $\mu_{crit}(J)$ which is the value of μ at which our solution for the given value of J disappears in a saddle-node bifurcation as we shall see.

First, to see that there is such a minimum for μ one has to remember that the dependence on μ comes through d and g [see Eq. (9)]. Equation (41) is

$$\frac{d'\sqrt{\mu}}{2}=I^J_{\pm}(c;\mu), \tag{42}$$

where we have explicitly written the dependence on μ of I which comes only from g. For small values of μ the minimum value of $c(R_0)$, c^J_{min}, is greater than V_J^{max} so that no solution exists. Increasing μ, the curve $c(R_0)$ approaches $V_J(R_0)$ but the integral $I^J_{\pm}(c)$ has a large value because the possible values of c are large, i.e., $c\approx V_J^{max}$. For this relatively small value of μ, Eq. (42) cannot be satisfied. Increasing μ we shall arrive to a situation where there is a solution. Increasing again μ, the minimum c^J_{min} decreases and we arrive to the region where the two solutions exist. For very large values of μ, the values of c approach V^J_{max}. In fact the plot $\mu=\mu(c,J)$ looks very similar to the plot $I=I^J_{\pm}(c)$ [see Fig. 6(b)]. Since μ is a parameter of the system we see that for $\mu>\mu_{crit}(J)$ there are two solutions (one stable and the other unstable) which collide and disappear by a saddle-node bifurcation at $\mu_{crit}(J)=\min_c \mu(c)$.

We can compute $\mu_{crit}(J)$ numerically or, equivalently, $J_{ph,cr}(\mu)$, which is depicted in Fig. 7. The stationary solu-

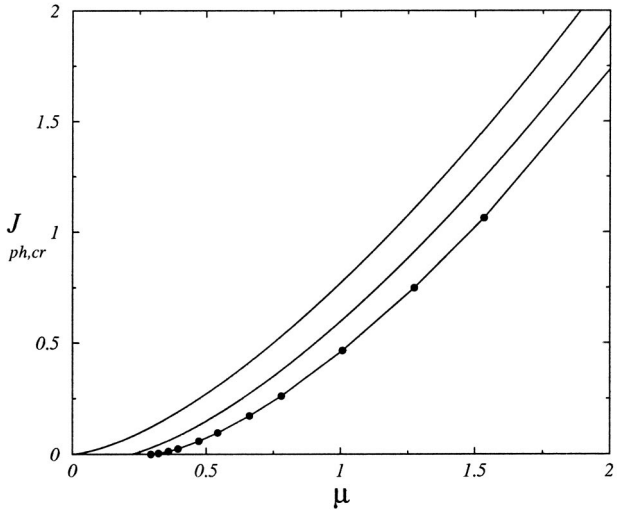

FIG. 7. Plot of the critical current as a function of μ. The quantities are in NLS units. Here $g'=0.3$ and $d'=1.0$. The curve with the dots represents the numerical results obtained by computing the minimum of $\mu(c)$ for different J. The upper (far) curve is the critical value for the current without the lattice [see Eq. (40)] while the near curve uses the approximation (44) for small g.

tion disappears by a saddle-node bifurcation when μ decreases down to $\mu_{crit}(J)$ or J increase up to $J_{ph,cr}(\mu)$.

For a small potential strength g, we can explicitly compute the first correction in g to the critical current (40). In fact in the limit $g\to 0$ the difference $R_m - R_0 \to 0$ and Eq. (38) gives

$$\frac{d}{2} = \frac{R_m - R_0}{\sqrt{c - V_J(R_0)}}. \tag{43}$$

From Eq. (36), $\sqrt{c - V_J(R_0)} = gR_0/2$. Considering $R_m - R_0$ small, we can expand $V_J(R_m)$ around R_0 up to first order in the difference $R_m - R_0$. From Eqs. (36) and (37) we get $R_m - R_0 = g^2 R_0^2/8[R_0 - R_0^3 - (J^2/4R_0^3)]$. Setting this equation into Eq. (43) and taking the limit $J \to J_q$, which means $R_0 \to R^* = \sqrt{2/3}$ [see after Eq. (40)] we finally obtain $J_{cr} = (4/3\sqrt{3})[1 - (3g/4d)]$ or in terms of the physical variables

$$J_{ph,cr} = \frac{4}{3\sqrt{3}} \mu^{3/2} \left(1 - \frac{3g'}{4d'\mu} \right), \tag{44}$$

which should hold asymptotically when $\mu \to \infty$. On the other hand, one may have an idea of the critical current in the limit case $g \to \infty$. From Eq. (36) one gets in this limit

$$R_0^2 = \frac{2c + \sqrt{4c^2 - J^2 g^2}}{g^2}.$$

One notes here that both R_0 and the current J scale as $1/g$; one expect then that as $g \to \infty$,

$$J_{cr} \sim 1/g. \tag{45}$$

These asymptotic behaviors are also observed for one isolated obstacle [6].

III. NONSTATIONARY SOLUTIONS

A. Sound

In this section we shall derive the long wave dynamics for the excitations around the ground state. Sound waves are the excitations with the lower energy. For the homogeneous solution of the NLS equation the excitation spectrum was obtained by Bogoliubov [1]. The excitation spectrum of a system under the action of an external periodic potential has been recently studied in Ref. [13]. In their treatment the potential is a very smooth function which allows them to consider the Thomas-Fermi approximation. In our case the potential is of very short variation and one cannot apply the Thomas-Fermi approximation. For simplicity we analyze this problem with Eqs. (3) and (4) which are equivalent to Eq. (1). We consider sound waves that propagate in the system as perturbations of the ground state, i.e.,

$$\rho = \rho_0(x) + \rho_1, \qquad \theta = -\mu t + \theta_1. \tag{46}$$

The equations that govern the sound waves are obtained setting Eq. (46) into Eqs. (3) and (4). Using the fact that the ground state satisfies Eq. (6)

$$\mu = \rho_0(x) + U - \frac{(\sqrt{\rho_0})_{xx}}{\sqrt{\rho_0}},$$

and keeping only the linear terms, these equations are

$$\partial_t \rho_1 = -2\partial_x(\rho_0 \partial_x \theta_1),$$

$$-\partial_t \theta_1 = \left(\frac{3}{2} - \frac{\mu - U}{2\rho_0} \right) \rho_1 - \frac{1}{2\sqrt{\rho_0}} \partial_{xx} \left(\frac{\rho_1}{\sqrt{\rho_0}} \right). \tag{47}$$

From these equations it is possible to study the excitation spectrum in detail. Since the ground state is a periodic function, this spectrum should display the typical band structures as follows from Bloch's theorem. Here we shall only obtain the long-wavelength part of the spectrum, in particular the effective sound speed. This allows us to neglect the high derivatives of ρ_1 because they contribute to the dispersion. After some simplifications the pair (47) leads to the equation

$$\partial_{tt} \rho_1 = +2\partial_x \{ \rho_0 \partial_x [W(x)\rho_1] \} \tag{48}$$

with

$$W(x) = 2 - \frac{\mu - U}{\rho_0} - \left[\frac{(\sqrt{\rho_0})_x}{\rho_0} \right]^2. \tag{49}$$

Since we are interested in the long-wavelength regime, we assume that there are two different length scales in the problem: the acoustic propagation is the large scale (X) and the lattice distance, i.e., the period of the ground state, is the small scale (x). Consequently, the function ρ_1 which appears in Eq. (48) has *a priori* dependence on X and x. We define the functions

$$\tilde{\alpha}(x) = \rho_0(x) W'(x) = \alpha_0 + \alpha(x), \tag{50}$$

$$\tilde{\beta}(x) = \rho_0(x) W(x) = \beta_0 + \beta(x), \tag{51}$$

where α_0 and β_0 are the mean values of $\tilde{\alpha}$ and $\tilde{\beta}$ and $\alpha(x)$ and $\beta(x)$ are the rapid variations of these functions (this implies that the mean values of α and β are zero). These functions do not depend on the large scale since the ground state fluctuates only over the small scale. The periodicity of ρ_0 implies the periodicity of $W(x)$ and, thus, both functions can be considered in the interval $x \in (0, d')$. As we noticed, the ground state is symmetric with respect to $x = d'/2$ so that ρ_0 is even with respect to $x = d'/2$ and therefore from Eq. (49) it follows that $W(x)$ is also even with respect to $x = d'/2$. As a consequence, we get from Eq. (50) that $\tilde{\alpha}$ is odd and thus $\alpha_0 = 0$ while $\tilde{\beta}$ is an even (always with respect to $x = d'/2$).

To solve Eq. (48) we use a method introduced by Kapitza, to calculate effective forces acting on an oscillator in the presence of a rapidly varying field [17]. We use a scaling where the slow variable X is related to the fast x through a big number K which is proportional to the ratio between the

sound wavelength and the period of the lattice, i.e., $K=\lambda/d'$. The spatial derivative is changed according to

$$\partial_x \rightarrow K\partial_x + \partial_X$$

and ρ_1 is replaced by

$$\rho_1 \rightarrow u_0(X) + \frac{u(x,X)}{K}.$$

After substitutions into Eq. (48), we get at the order $\mathcal{O}(K^1)$ the equation

$$\alpha' u_0 + \beta_0 u_{xx} + \beta' u_0' + \beta' u_x + \beta u_{xx} = 0 \tag{52}$$

and at the order $\mathcal{O}(K^0)$

$$-\omega^2 u_0 = 2(\alpha' u + \alpha u_x + 2\beta_0 u_{xX} + \alpha u_0' + \beta_0 u_0'' + \beta u_0'' + \beta' u_X + 2\beta u_{xX}). \tag{53}$$

We have denoted the derivative of the function by a symbol $'$ where no confusion arises. Equation (52) is an equation for the fast variations of u. The last two terms of Eq. (52) are products of two rapidly varying functions so that they vary at different scales and they are thus neglected [17]. Thereafter Eq. (52) can be integrated directly and we obtain

$$u(x,X) = -\frac{1}{\beta_0}\left(u_0(X)\int \alpha(x)dx + u_0'(X)\int \beta(x)dx \right). \tag{54}$$

Replacing this result in Eq. (53) gives

$$-\frac{\omega^2}{2}u_0 = -u_0'\left(\alpha + 3\frac{\alpha\beta}{\beta_0} + \frac{\alpha'}{\beta_0}\int \beta + \frac{\beta'}{\beta_0}\int \alpha \right) - u_0\left(\frac{\alpha'}{\beta_0}\int \alpha + \frac{\alpha^2}{\beta_0} \right) + u_0''\left(\beta_0 - \beta - \frac{2\beta^2}{\beta_0} - \frac{\beta'}{\beta_0}\int \beta \right).$$

Now we proceed to take the average of this equation. After some algebra and remembering that the product $\alpha\beta$ is odd and of zero mean value we get that the first and second terms have zero average. Only the third term has a nonzero average. Supposing $u_0 \sim \exp(iqX)$ and denoting the average by $\langle\cdot\rangle$, we get for the effective sound speed c_{eff}

$$c_{eff}^2 = 2\beta_0\left(1 - \frac{\langle\beta^2\rangle}{\beta_0^2} \right).$$

As a particular case we see that without periodic potential $\rho_0=\mu$ and thus $\beta_0=\rho_0$ and $\langle\beta^2\rangle=0$, i.e., $c_{eff}=\sqrt{2\rho_0}$ as it should be.

We compute the effective sound speed in the limit $g \rightarrow 0$. In this limit, at the lowest order we get

$$c_{eff} = \sqrt{2\mu} + O(g').$$

On the other hand, one may compute c_{eff} near μ_c using the same approximation as the one used to compute Eq. (31), which is the low-density regime. After some algebra one gets

$$c_{eff}^2 \sim \mu c(\mu) \xrightarrow[\mu\rightarrow\mu_c]{} 0.$$

Note that at very low density the sound speed vanish because $c(\mu_c)=0$.

B. Saddle-node transition

After the saddle-node transition, no superflow solution exists in the lattice. We numerically solve the NLS equation in order to explore the time-dependent solutions (see Fig. 8). As the current crosses the threshold, gray solitons are periodically emitted from the obstacle as was observed in [6]. They travel at a given speed until they arrive to the next obstacle and are partially transmitted and reflected. At the same time, sound waves propagate in the system creating interferences. In Fig. 8 we show consecutive snapshots of the temporal evolution. In Fig. 8(a) the flow is already present in the system. The absolute value of the wave function at the deltas is decreasing on time. Figures 8(b) and 8(c) show, respectively, the amplitude just before and after the gray soliton is nucleated at the delta potentials. The soliton propagates downstream at a constant velocity until it reaches the next delta potential. During this time other solitons could have been nucleated. Figure 8(d) shows two solitons propagating inside each unit cell. After the scattering of the first soliton with the delta potentials a fraction is transmitted and other reflected. Since their amplitude is smaller they travel faster generating a complex dynamics of interferences with other solitons and sound waves. We have observed a very rich behavior but we shall not enter into detail since this is a problem that will be addressed in a separate paper.

IV. GENERAL REMARKS AND CONCLUSIONS

A. Superfluid λ transition in a lattice

Let us consider the Ginzburg-Landau free energy for the superfluid λ transition [2] near T_λ

$$F = \int \left(\frac{\hbar^2}{2m}|\psi_x|^2 - \mu(T)|\psi|^2 + \beta(T_\lambda)\frac{|\psi|^4}{2} + U(x)|\psi|^2 \right) dx. \tag{55}$$

Here ψ is the order parameter, $\mu(T)=\alpha(T_\lambda - T)$ and $\beta(T_\lambda)$ are constants depending only on the thermodynamic variables. Without an external field (the periodic lattice), one has a second-order phase transition as the temperature decreases below T_λ. In the presence of a boundary condition, this threshold changes (see Ginzburg and Pitaevskiĭ [2]). Our study shows that this effect remains in the presence of an external periodic lattice. In fact, the computations are the same as in Sec. II A 1 where we have computed the ground-state solution (it is the periodic solution). The existence of a nonzero wave function is possible if the relation

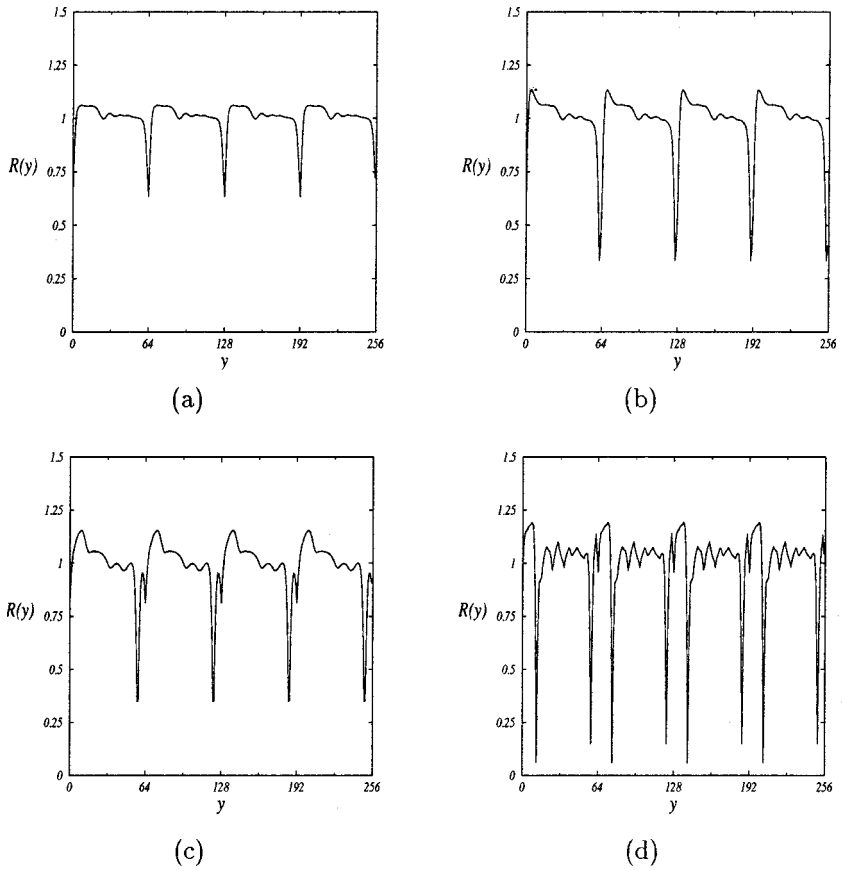

FIG. 8. Temporal evolution of gray soliton emission: (a) $t=2.1$, (b) $t=9.2$, (c) $t=10.3$, (d) $t=21.1$. Here $g'=0.3$ and $d'=64$ mesh points, the mesh size dy being equal to 1. The flow (from right to left) is imposed by a Galilean boost to NLS by adding a $2iv\partial\psi$ to Eq. (1). This boost fixes an external current J. As the flow (that is the current) increases one sees that the steady state breaks down to a temporal one where gray solitons [the big depletion near the left-hand side of each point 64, 128, and 192 in (c)] are emitted taking some energy. See main text for details. The quantities are in NLS units.

$$\tan\left(\frac{\sqrt{2m\mu(T)}d'}{2\hbar}\right)\geqslant\frac{\sqrt{2m}g'}{2\sqrt{\mu(T)}\hbar} \tag{56}$$

holds. This relation follows directly from Eq. (29) but with a given value of μ in the present context. This gives a shift in the critical temperature in the superfluid transition because of the lattice. Two limits are easy to consider.

(i) For small g', one approximates the function $\tan(x)$ by its linear part ($\approx x$); that is, $d'=g'/\mu(T)=g'/\alpha(T_\lambda-T)$, which gives the critical temperature

$$T_c=T_\lambda-\frac{g'}{\alpha d'}.$$

In this limit the critical temperature decreases as the lattice-superfluid interaction increases. It happens that it is possible to prove that Eq. (56) is also valid for $g<0$. It is interesting to note that an attractive interaction with the lattice increases the critical temperature.

(ii) As $g'\to\infty$, one has that the argument of the tangent function reaches $\pi/2$, so that $\pi\hbar=d'\sqrt{2m\mu(T)}$, which gives the following shift for the critical temperature:

$$T_c=T_\lambda-\frac{\hbar^2\pi^2}{2m\alpha d'^2}.$$

Even if those relations are only valid for temperatures near the λ point they suggest that some crystal structures or superlattices could destroy the superfluidity and /or superconductivity because they would shift the transition temperature down to 0 K.

B. Convexity of the energy and properties of degeneracy and zeroes of the ground state

As we have said the ground-state solution has no zero. Moreover, it is nondegenerate in the sense that $R_0(y)$ and $-R_0(y)$ represent the same state. Those properties follow directly from a general property of the functional $E[R]$ for the pure real field $R(y)$ defined in Eq. (21). This property is the following: the functional energy $E[R]$ is convex in R^2. That is, for any real λ such that $0\leqslant\lambda\leqslant1$, then

$$E[R^2=\lambda R_1^2+(1-\lambda)R_2^2]\leqslant\lambda E[R_1^2]+(1-\lambda)E[R_2^2].$$

Here $R_1(y)$ and $R_2(y)$ are two real functions. The proof of this property requires only that $\int dy\,R_y^2$ is convex because both $\int dy(R^4/2)$ and $\int dy\,U(y)R^2$ are clearly convex. The convexity of $\int dy\,R_y^2$ follows after a proof by Benguria and collaborators [18]. We sketch this proof in the following lines.

Let $R^2=\lambda R_1^2+(1-\lambda)R_2^2$, then one has that (primes denote derivative respect to y)

$$RR'=\lambda R_1R_1'+(1-\lambda)R_2R_2'.$$

Now we use the Cauchy-Schwarz inequality: $(a_1b_1+a_2b_2)^2\leqslant(a_1^2+a_2^2)(b_1^2+b_2^2)$ with $a_1=\sqrt{\lambda R_1}$, $b_1=\sqrt{\lambda R_1'}$, $a_2=\sqrt{(1-\lambda)R_2}$, and $b_2=\sqrt{(1-\lambda)R_2'}$. Then one has

$$R^2 R'^2 \leqslant [\lambda R_1^2 + (1-\lambda) R_2^2][\lambda R'^2_1 + (1-\lambda) R'^2_2],$$

which proves the convexity of $\int dy\, R_y^2$ in R^2 whenever R^2 does not vanish.

One has the following property: If $E[R^2]$ is convex then the ground state R_0^2 which minimizes $E[R^2]$ is not degenerated and has no nodes.

The proof of this statement follows in two parts.

(i) We shall prove the reciprocate, that is, if the ground state R_0^2 is degenerate then $E[R^2]$ is not convex. If R_1^2 and R_2^2 are two different ground states then one has that $E[R_1^2] = E[R_2^2]$ are two absolute minima, but this means that $E[R^2]$ could not be convex because convexity would imply the existence of an ''intermediate'' solution $[R^2 = \lambda R_1^2 + (1-\lambda) R_2^2]$ with a lower energy; therefore, R_1^2 and R_2^2 are not the ground state, or, if they are, one has that $R_1^2 = R_2^2$.

(ii) Similarly, we show that if the ground state R_0^2 has a node then $E[R^2]$ is not convex. Let $R_0(y)$ be the ground state with a node at y_0 and $E[R_0^2]$ is the absolute minimum of $E[R^2]$. Near the node $R_0(y)^2$ behaves locally as $R_0^2 \approx \alpha^2 (y-y_0)^2$. Following an argument due to Feynman [19] one may see that a function $R_F(y)$, consisting of the same $R_0(y)$ but with a local modification near $y \approx y_0$ of the form $[R_F(y)]^2 \approx \Delta + \alpha^2 (y-y_0)^2$, possesses less total energy. This is impossible in a convex energy and contradicts also the fact that R_0 is a minimum of the functional. Q.E.D.

C. Conclusion

We have studied the stationary solutions of the defocusing NLS equation in a periodic potential, namely the Kronig-Penney potential. We have characterized the ground state, the excited states, and the steady flows. These ''real excitations'' can be characterized with the help of a Poincaré map and they turn out to be typically periodic, quasiperiodic, or chaotic in space. We have also studied some simple dynamical behaviors like sound propagation in a periodic ground state.

Finally, we have shown that the steady-flow solution does not exist for any value of the parameters. For fixed external parameters such as the lattice strength, the period of the potential, and the total number of particles per cell (g', d', N), the steady-flow solution disappears by a saddle-node bifurcation as the current (J) increases. This transition is analogous with the one observed in infinite spatially extended systems governed by the NLS equation [5,6]. We have obtained the approximate dependence of the critical current in the limit of small and large values of g' [see Eqs. (44) and (45)]. These have the same behaviors as obtained in [6] for the case of one delta potential and can be interpreted as the effect of the coherence on the wave function.

ACKNOWLEDGMENTS

We thank Professor G. Nicolis for support and encouragement in this research. We also acknowledge R. Benguria, M. E. Brachet, P. Coullet, and V. Hakim for useful discussions. F.B. is financially supported by the ''Communauté française de Belgique'' and P.G. by the National Fund for Scientific Research (FNRS, Belgium). This research is financially supported in part by the Training and Mobility Program of the European Commission, and by the Interuniversity Attraction Pole program of the Belgian Federal Office of Scientific, Technical and Cultural Affairs. Part of this work was done in Santiago de Chile under the support of Contract No. ECOS-Conicyt.

[1] N.N. Bogoliubov, J. Phys. Radium **11**, 23 (1947).

[2] V.L. Ginzburg and L.P. Pitaevskiĭ, Zh. Éksp. Teor. Fiz. **34**, 1248 (1958) [Sov. Phys. JETP **7**, 858 (1958)]; L.P. Pitaevskiĭ, *ibid.* **40**, 646 (1961) [*ibid.* **13**, 451 (1961)]; E.P. Gross, J. Math. Phys. **4**, 195 (1963).

[3] M.H. Anderson, J.R. Ensher, M.R. Mathews, C.E. Wieman, and E. Cornell, Science **269**, 198 (1995); C.C. Bradley, C.A. Sackett, J.J. Tollet, and R.G. Hulet, Phys. Rev. Lett. **75**, 1687 (1995); K.B. Davis, M.O. Mewes, M.R. Andrews, N.J. Van Druten, D.D. Durfee, D.M. Kum, and W. Ketterle, *ibid.* **75**, 3969 (1995).

[4] M.R. Andrews, D.M. Kum, H.-J. Miesner, D.S. Durfee, C.G. Townsend, S. Inouye, and W. Ketterle, Phys. Rev. Lett. **79**, 553 (1997); **80**, 2697 (1997).

[5] T. Frisch, Y. Pomeau, and S. Rica, Phys. Rev. Lett. **69**, 1644 (1992).

[6] V. Hakim, Phys. Rev. E **55**, 2835 (1997).

[7] C. Raman, M. Kóhl, R. Onofrio, D.S. Durfee, C.E. Kuklewicz, Z. Hadzibabic, and W. Ketterle, Phys. Rev. Lett. **83**, 2502 (1999).

[8] A.C. Newell and J.V. Moloney, *Nonlinear Optics* (Addison-Wesley, Redwood City, CA, 1992).

[9] G. Lenz, P. Meystre, and E.M. Wright, Phys. Rev. Lett. **71**, 3271 (1993).

[10] W. Zhang, D.F. Walls, and B.C. Sanders, Phys. Rev. Lett. **72**, 60 (1994).

[11] W. Zhang and D.F. Walls, Phys. Rev. A **49**, 3799 (1994).

[12] S. Aubry and P.Y. Le Daeron, Physica D **8**, 381 (1983).

[13] K. Berg-Sorensen and K. Molmer, Phys. Rev. A **58**, 1480 (1998).

[14] G.D. Birkhoff, Acta Math. **50**, 359 (1927); Mem. Pont. Acad. Sci. Novi. Lyncaei **1**, 85 (1935).

[15] V. I. Arnold, *Equations Différentielles Ordinaires* (Editions MIR, Moscow, 1974).

[16] This integral can be written in the form

$$\int \frac{dy}{\sqrt{4y^3 - g_2 y - g_3}}$$

which defines the elliptic $\mathcal{P}$-Weierstrass function.

[17] L.D. Landau and E.M. Lifshitz, *Mécanique, Physique Théorique* (Editions MIR, Moscow, 1974), Vol. I.

[18] R. Benguria, Ph.D. thesis, Princeton University, 1979 (unpublished); R. Benguria, H. Brezis, and E.H. Lieb, Commun. Math. Phys. **79**, 167 (1981).

[19] R.P. Feynman, *Statistical Mechanics* (Addison-Wesley, Reading, MA, 1972).